J|A|C|S COMMUNICATIONS

Published on Web 07/24/2009

Facile Synthesis of Superparamagnetic Fluorescent Fe_3O_4/ZnS Hollow Nanospheres

Zhenxuan Wang, Limin Wu,* Min Chen, and Shuxue Zhou

Department of Materials Science and Advanced Materials Laboratory, Fudan University, Shanghai 200433, China

Received April 22, 2009; E-mail: lmw@fudan.edu.cn

Core−shell and hollow nanospheres (NSs) have attracted tremendous interest in recent research.[1] One reason is that they can be used for targeted drug delivery by controlling the organization of different functional nanoparticles into NSs.[2] One preparation strategy is to use porosified silica as a robust shell to coat functional nanoparticles,[3] but some inherent limitations exist in this method, such as low particle loading.[4] Another approach involves the direct construction of hollow NSs (HNSs) from functional building blocks, such as CoPt,[5a] $CoSe_2$,[5b] Fe_3O_4,[5c] and α-Fe_2O_3[5d] HNSs, using processes such as the Kirkendall effect,[5e] preferential dissolution,[5f] and acid etching.[5g] However, all of the HNSs reported are monocomponent and need to be further functionalized by introduction of other components, which poses some other difficulties, such as ensuring a stable coating of the desired materials on the surface of the HNSs and preventing the clogging of pores.[6] Therefore, finding a facile way to simultaneously construct multiple functionality into HNSs still remains a big challenge.

Here we report for the first time the successful synthesis of superparamagnetic fluorescent Fe_3O_4/ZnS HNSs with diameters of <100 nm using a simple method that we call corrosion-aided Ostwald ripening. The synthetic procedure is very easy and straightforward. When the synthesized monodisperse FeS particles were dispersed in a mixture containing zinc acetylacetonate (ZA), poly(vinylpyrrolidone) (PVP), ammonium nitrate, glycol, and water and then reacted at 150 °C for 10 h, the Fe_3O_4/ZnS HNSs were directly obtained. A large-scale view (Figure 1a) indicates that the as-synthesized NSs have typical hollow structure with average internal and external diameters of 66 and 97 nm, respectively. The high-resolution transmission electron microscopy (HRTEM) image (Figure 1b) reveals that the shell is composed of close-packed light and dark particles that have regions oriented in the outer and inner layers, respectively. The particles have interplanar spacings of 0.312 and 0.486 nm (upper-left inset in Figure 1b), corresponding to the (111) planes of cubic ZnS and Fe_3O_4, respectively. The selected-area electron diffraction (SAED) rings (bottom-right inset in Figure 1b) can be assigned to superposition of the diffraction patterns of polycrystalline Fe_3O_4 and ZnS. Energy-dispersive X-ray (EDX) analysis further confirmed that the internal shell mainly consists of Fe and O and the external shell of Zn and S [Figure S1 in the Supporting Information (SI)]. The TEM images (Figure 1c−f) and corresponding changes in the outer diameter (Figure S2 in the SI) provide a time-dependent insight into the formation of these HNSs. The FeS particles (Figure 1c) were uniform with a mean diameter of 66 nm and a hexagonal phase inferred from XRD analysis (JCPDS No. 80-1026; Figure S3 in the SI). After reaction for 2 h, there were particles surrounding the FeS particles (Figure 1d), and after 4 h, the outer particles aggregated to form a shell (Figure 1e). Meanwhile, the core size gradually decreased, as the small particles under the building shell faded out and the void between core and shell increased. As the solid evacuation continued, the core further decreased in size (Figure 1f). The XRD data confirmed that the emerging phases at intermediate reaction times could be attributed to ZnS (JCPDS No. 77-2100) and Fe_3O_4 (JCPDS No. 86-1354) (Figure S3 in the SI). Reaction for 10 h yielded complete HNSs with a polycrystalline nature consisting of ZnS and Fe_3O_4 according to the XRD data (Figure S3 in the SI). Fe_3O_4 and ZnS particles were equal in size at different stages: the mean sizes were 5 and 7.6 nm at reaction times of 4 and 10 h, respectively. Disappearance of the FeS fraction indicates a complete conversion of the FeS phase in the core.

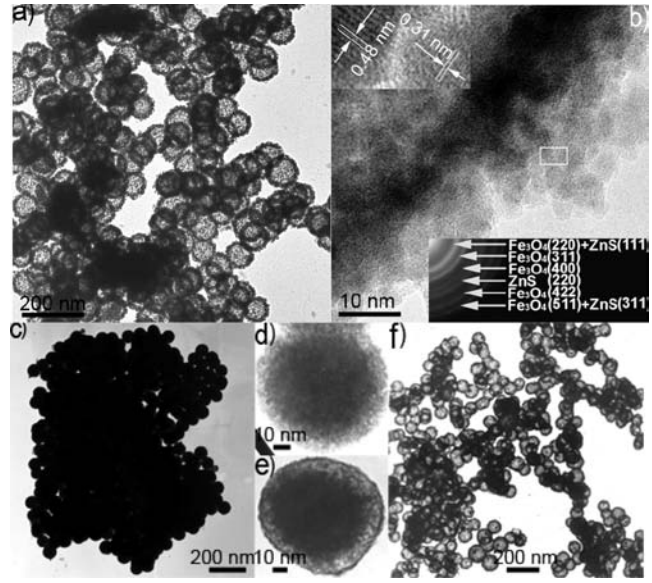

Figure 1. (a) TEM image of the Fe_3O_4/ZnS HNSs. (b) HRTEM image, SAED pattern (bottom-right inset) of the HNSs shell, and inserted image of the interface area [white rectangle] between Fe_3O_4 and ZnS particles (upper-left inset). (c) FeS particles and the samples from subsequent reaction at 150 °C for (d) 2 h, (e) 4 h, and (f) 6 h.

Two control experiments were carried out in which half of the ZA volume was added or ZA was excluded, generating half-hollow (Figure S4 in the SI) and intact FeS particles, respectively. This suggests that FeS particles act as "in situ" templates and ZA as an etching agent. From the above discussion, we deduced a possible HNS formation mechanism (Figure 2). ZA hydrolysis at pH 6−9 generates $Zn(NH_3)_4(OH)_2$,[7] which further erodes the added FeS particles (Figure 2a) to create a supersaturated Fe_3O_4[8] and ZnS phase. This phase undergoes consequent nucleation and growth around the entire surface stabilized by PVP (Figure 2b). This granular layer around the FeS particles completely hinders a direct chemical reaction between FeS and ZA, and thus, the Kirkendall effect cannot explain the subsequent formation of the hollow structure. Since there is a net positive charge on the surfaces of FeS[9a] and ZnS[9b] particles but a negative charge on Fe_3O_4[9a] at pH 6.2−6.9, the preferred location of Fe_3O_4 and ZnS particles can be attributed to positional adjustment due to electrostatic interactions. As time passes, FeS, ZA, and water are gradually consumed, and the resultant ZnS and Fe_3O_4 molecules decrease, as does the growth

10.1021/ja903246e CCC: $40.75

rate because of the narrowing concentration gap between the molecules in the medium and the equilibrium value needed for growth.[10] Ostwald ripening occurs as the Fe_3O_4 and ZnS around the surface of the FeS form small particles that grow into larger particles and then coalesce to form a shell (Figure 2c).[2b] Etching does not cease until the FeS core has vanished, finally leaving Fe_3O_4/ZnS HNSs (Figure 2d). Since the total mass increases in going from the FeS template to the final Fe_3O_4 and ZnS structure, the overall HNS diameter increases. This is different from previous reports,[11] in which the particle size does not change much because the total mass does not vary.

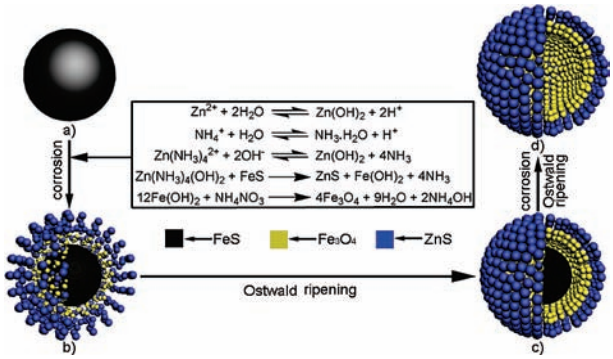

Figure 2. Schematic diagram of the formation of Fe_3O_4/ZnS HNSs.

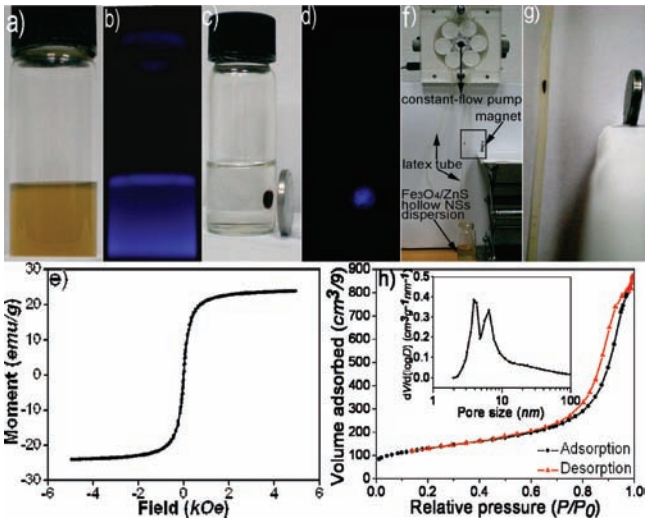

Figure 3. (a) Visual image and (b) afterglow of HNSs dispersed in PBS. (c) Visual photograph and (d) afterglow of aggregated HNSs captured by a magnet. (e) Magnetic-field dependence at room temperature. (f) In vitro apparatus to mimic human circulation and (g) enlarged image of the target site (rectangle in f). (h) N_2 adsorption/desorption isotherms (inset: pore size distribution).

The as-produced Fe_3O_4/ZnS HNSs were isolated and homogeneously redispersed into phosphate-buffered saline (PBS) (Figure 3a). This dispersion emitted a visible blue afterglow even 18 min after the UV irradiation source (365 nm) was removed (Figure 3b). Several quantitative investigations showed that the HNSs had a quantum yield of 13% and a photoluminescence (PL) emission spectrum with a maximum at 431 nm and long afterglow behavior (Figure S5 in the SI). The HNSs took only several minutes to accumulate near an external magnetic field (Figure 3c). The aggregates also emitted a bright blue afterglow (Figure 3d). The negligible coercivity and remanence in the magnetization curve (Figure 3e) as well as the zero-field cooling and field cooling modes (Figure S6 in the SI) indicate that these HNSs exhibit superparamagnetic behavior. Figure 3f shows a simple in vitro apparatus for simulation of a targeted guide in human circulation. An external magnetic field was applied to retain HNSs at a target site (Figure 3g). This behavior ended after 10 min when the volume and reflux rate of the sample suspension were respectively set to 10 mL and 5 cm s^{-1} (10 times faster than capillary blood flow), and the HNS retention rate was as high as 92% even at a low magnetic field strength of 0.12 T. Moreover, the Fe_3O_4/ZnS HNSs are mesoporous because of the typical feature of Ostwald ripening.[11] N_2 adsorption/desorption measurements (Figure 3h) demonstrated that the HNSs have a BET surface area of 1016 m^2 g^{-1}. Two central pore distributions are evident, one at 3.6 nm and another 4.8 nm (Figure 3h inset), which can be attributed to the different packing densities in the Fe_3O_4 and ZnS layers. A 3-(4,5-dimethylthiazol-2-y1)-2,5-diphenyltetrazolium bromide assay was used to evaluate cell viability. After HNS incubation with HeLa cells for 48 h, there were no signs of toxicity even up to doses of 50 μM (Figure S7 in the SI).[12] Further delivery experiments for the anticancer agent doxorubicin (Figure S8 in the SI) revealed a loading of 13.8% and a release rate comparable to that of conventional silica drug carriers.[6] The HNSs seem to aggregate because of insufficient PVP addition. This problem could be solved by surface modification.

In summary, we have presented a very simple strategy for the synthesis of HNSs with both superparamagnetic and fluorescent properties. When monodisperse FeS particles were dispersed in a mixture containing ZA, PVP, ammonium nitrate, glycol, and water and treated at 150 °C for 10 h, superparamagnetic and fluorescent Fe_3O_4/ZnS HNSs were directly obtained. Neither further loading nor subsequent reaction with functional components was needed. These multifunctional HNSs or modified particles thereof have potential for exciting applications in biomedicine, such as targeted drug delivery, integrated imaging, diagnosis, and therapeutics. Many other multifunctional HNSs could also be obtained using this approach.

Acknowledgment. This work was supported by the Foundation of STS (07DJ14004), Shanghai Leading Academic Disciplines (B113), and Shuguang Scholar-Tracking Foundation.

Supporting Information Available: Experimental section, TEM images, EDX and XRD data, PL spectrum, $M-T$ curve, doxorubicin release curve, and complete ref 5f. This material is available free of charge via the Internet at http://pubs.acs.org.

References

(1) Yin, Y.; Rioux, R. M.; Erdonmez, C. K.; Hughes, S.; Somorjai, G. A.; Alivisatos, A. P. *Science* **2004**, *304*, 711.
(2) (a) Ferrari, M. *Nat. Rev. Cancer.* **2005**, *5*, 161. (b) Liu, B.; Zeng, H. *Small* **2005**, *1*, 566.
(3) Yi, D. K.; Selvan, S. T.; Lee, S. S.; Papaefthymiou, G. C.; Kundaliya, D. J.; Ying, Y. *J. Am. Chem. Soc.* **2005**, *127*, 4990.
(4) Zhao, W.; Gu, J.; Zhang, L.; Chen, H.; Shi, J. *J. Am. Chem. Soc.* **2005**, *127*, 8916.
(5) (a) Vasquez, Y.; Sra, A. K.; Schaak, R. E. *J. Am. Chen. Soc.* **2005**, *127*, 12504. (b) Gao, J.; Zhang, B.; Zhang, X.; Xu, B. *Angew. Chem., Int. Ed.* **2006**, *45*, 1220. (c) Peng, S.; Sun, S. *Angew. Chem., Int. Ed.* **2007**, *46*, 4155. (d) Bang, J. H.; Suslick, K. S. *J. Am. Chem. Soc.* **2007**, *129*, 2242. (e) Gao, J.; Liang, G.; Cheung, J. S.; Pan, Y.; Kang, Y.; Zhao, F.; Zhang, B.; Zhang, X.; Wu, E. X.; Xu, B. *J. Am. Chem. Soc.* **2008**, *130*, 11828. (f) Jia, C.; et al. *J. Am. Chem. Soc.* **2008**, *130*, 16968. (g) An, K.; Kwon, S. G.; Park, M.; Na, H. B.; Baik, S.; Yu, J. H.; Kim, D.; Son, J. S.; Kim, Y. W.; Song, I. C.; Moon, W. K.; Park, H. M.; Hyeon, T. *Nano Lett.* **2008**, *8*, 4252.
(6) Lou, X.; Archer, L. A. *Adv. Mater.* **2008**, *20*, 1853.
(7) Le, H.; Chua, S. *Appl. Phys. Lett.* **2005**, *87*, 101908.
(8) (a) Sugimoto, T.; Matijević, E. *J. Colloid Interface Sci.* **1980**, *74*, 227. (b) Carsley, S. H. *J. Phys. Chem.* **1930**, *34*, 178.
(9) (a) Toro, D. M. D.; Mahony, J. D.; Gonzalez, A. M. *Environ. Toxicol. Chem.* **1996**, *15*, 2156. (b) Feldmann, C.; Merikhi, J. *J. Colloid Interface Sci.* **2000**, *223*, 229.
(10) Madras, G.; McCoy, B. J. *Chem. Eng. Sci.* **2002**, *57*, 3809.
(11) Li, J.; Zeng, H. *J. Am. Chem. Soc.* **2007**, *129*, 15839.
(12) Manzoor, K.; Johny, S.; Thomas, D.; Setua, S.; Menon, D.; Nair, S. *Nanotechnology* **2009**, *20*, 065102.

JA903246E